J Nanopart Res (2016) 18:217
DOI 10.1007/s11051-016-3533-8

RESEARCH PAPER

How to determine the morphology of plasmonic nanocrystals without transmission electron microscopy?

Yann Battie · Irene Izquierdo-Lorenzo · Amandine Resano-Garcia · Aotmane En Naciri · Suzanna Akil · Pierre Michel Adam · Safi Jradi

Received: 16 March 2016 / Accepted: 25 July 2016 / Published online: 2 August 2016

Abstract This paper reports the complete ellipsometric characterization of gold nanoparticles (NPs) embedded in a photoresist films. The effective dielectric function of nanocomposite films as well as the shape distribution and the volume fraction of NPs are extracted from ellipsometric measurements by introducing an effective medium theory which takes into account the NP shape distribution and the intrinsic confinement effect. This theory remains valid as long as the nanoparticle interaction is negligible. We show that the magnitude of the confinement depends on the nanoparticle shape and the environment through chemical damping. This suggests that the NP shape distribution can be directly estimated by ellipsometry, while the determination of absolute radius distribution requires transmission electron microscopy measurements. The imaginary part of the effective dielectric function exhibits a strong asymmetric surface plasmon band, while a large variation of the real part occurs close to the resonance. The redshift and the broadening of the plasmon band as the gold volume fraction increases are correlated to the evolution of NP shape distribution. This evolution is attributed to a competition between the nucleation and the coalescence of NPs. This unambiguously demonstrates that ellipsometry combined with a shape-distributed effective medium theory is a powerful alternative tool to transmission electron microscopy for the NP shape analysis.

Keywords Nanoparticles · Shape distribution · Spectroscopic ellipsometry · Plasmon · Confinement · Instrumentation

Y. Battie (✉) · A. Resano-Garcia · A. E. Naciri · S. Akil
LCP-A2MC, Institut Jean Barriol, Université de Lorraine, 1 Bd Arago, 57070 Metz, France
e-mail: yann.battie@univ-lorraine.fr

I. Izquierdo-Lorenzo · P. M. Adam · S. Jradi
LNIO (CNRS UMR 6279), Université de Technologie de Troyes, 12 rue Marie Curie, 10010 Troyes, France

Introduction

Plasmonic nanoparticles (NPs) embedded in polymer matrices are remarkable composites mainly for their unique optical properties (Biswas et al. 2004; Kinnan et al. 2009; Pacios et al. 2007; Qu et al. 2004; Sandu 2012), which lead to their application as filters, blackbody, or optical sensors (Aldeanueva-Potel et al. 2009; Gradess et al. 2009; Hedayati et al. 2011; Liu et al. 2009; Misra et al. 2015; Pandey et al. 2012), but they have also proven enhanced conductivity (Kuila et al. 2007; Reddy et al. 2008; Takele et al. 2006), luminescence (Guzatov et al. 2012; Yang et al. 2012), and further worth as antibacterial agents (Kubacka et al. 2009; Tamboli et al. 2012). Usually, these materials are characterized by UV–visible spectroscopy, as the plasmon resonance (SPR) of NPs provides qualitative information on the NP load,

size, shape, and distribution. However, in order to establish these parameters precisely, transmission electron microscopy (TEM) studies are required. Even then, the optical characterization of the material is limited using this technique, as it is blind to the elucidation of its refractive index.

Spectroscopic ellipsometry (Azzam and Bashara 1977) is an indirect optical characterization tool based on the change of the polarization state of light after reflection on the sample. Ellipsometry requires an appropriate modeling to simultaneously determine the film thickness and dielectric constant. Recent works suggest that ellipsometry can be used to characterize nanomaterials (Losurdo et al. 2009; Naciri et al. 2013; Oates et al. 2011). Ellipsometry was previously used to monitor the growth of silver NPs on a surface (Oates and Mücklich 2005), in polymer (Oates 2006; Oates and Christalle 2007), or in mesoporous silica matrices (Battie et al. 2011). However, classical effective medium theories, used to exploit ellipsometric data, only consider monodispersed NPs and could give erroneous results (Keita and Naciri 2011). Pecharroman et al. (2015) used the Bergman formalism to extract the effective dielectric function of gold nanoparticules in TiO_2. The Bergman formalism is based on the determination of the spectral representation function (SRF) which depends on a large number of parameters such as the NP size and shape distributions, or the interactions between NPs. This multivariate dependence makes unclear the interpretation of the SRF. Persechini et al. (2014) have introduced the nanoparticle shape in effective medium theory to exploit reflectance anisotropy spectroscopic measurements. However, the authors consider monodispersed NPs. In addition, contrary to ellipsometry, reflectance anisotropy spectroscopic measurement is limited to oriented NPs. Recent advances in effective medium theory make it possible to take into account the influence of the NP size (Battie et al. 2014b; Keita et al. 2014) or shape distribution (Battie et al. 2014a, 2015; Bohren and Huffman 1998; Gao and Li 2003; Goncharenko 2003, 2004; Goncharenko et al. 2001; Goncharenko and Pinchuk 2014; Goncharenko and Venger 2004; Resano-Garcia et al. 2015; Toudert et al. 2008, 2012) on the optical properties of films. An extension of effective medium theories was developed by Toudert et al. (2008, 2012) to describe the optical properties of a collection of NPs distributed in shape and assembled into a 2D array. However, this model requires a preliminary estimation of the pair correlation function of NPs by transmission electron microscopy. By considering mean field approximation, Bohren and Huffman (1998) have introduced the NP shape distribution in the Maxwell–Garnett theory. By assuming a low NP volume fraction, a spectral Bergman representation can be derived from this shape-distributed effective medium theory (SDEMT) (Goncharenko 2004). By combining mean field approximation and the Bruggeman theory, Goncharenko and Venger (2004) have investigated the influence of the NP shape distribution on their percolation threshold. However, these authors consider unphysical distributions such as uniform step-like shape distribution. SDEMT was successfully exploited to analyze the absorption spectra of colloids (Battie et al. 2015; Resano-Garcia et al. 2015). However, contrary to ellipsometry, absorption spectroscopy is not sensitive to the real part of the complex dielectric function of NPs.

This paper reports the first complete ellipsometric determination of the NP shape distribution of gold NPs embedded in a photoresist matrix. The aim behind the use of this resist is to develop metamaterials based on 3D metallic structures using 3D lithography. Based on a direct laser writing in a metallic precursor-loaded a photoresist solution, 3D metallic metamaterials can be obtained (Destouches et al. 2013; Ishikawa and Tanaka 2012; Shukla et al. 2011). In this context, ellipsometry was used to get the optical properties and in particular the dielectric constant of gold NPs embedded in thin polymer films. It is interesting to note that in the present study, the NPs were thermally fabricated to obtain similar NP properties as in photopatterned structure. Indeed, as we used a positive photoresist, the areas exposed to light are removed after the photolithographic step while the reduction of Au precursor and the growth of AuNPs inside the unexposed areas require a postannealing treatment. The ellipsometric data are analyzed using the SDEMT model. In agreement with TEM, the NP shape estimated from ellipsometry evolves from spherical to nonspherical NPs as the gold concentration increases. This variation, which comes from a competition between the nucleation and the coalescence of NPs, has a significant impact on the complex dielectric function. It induces a red shift and a broadening of the plasmon resonance. This demonstrates that ellipsometry can be used to simultaneously estimate the NP

shape distribution and the complex dielectric function of nanocomposite films.

Materials and methods

Synthesis of the Au@AZ9260 composites

As a test material, we present a nanocomposite that includes AuNPs inside a well-known photosensitive prepolymer which may still be used as two-photon lithography resist, as the similar composites prepared by Marques-Hueso et al. (2010). The AuNPs in the composite were generated in situ, reducing $HAuCl_4$ by the cresol novolac resist present in the AZ9260 commercial preparation. For each AuNP load level, weighted solutions of $HAuCl_4{\cdot}3H_2O$ in propyleneglycol monomethyl ether acetate (PGMEA) were added to the corresponding amount of commercial AZ9260. The mixtures were homogenized in an ultrasonic bath for 1 min at room temperature. Immediately after preparation, they were spin coated over a silicon substrate at 5000 rpm for 60 s. Cleaned transparent glass substrates are also used for absorption spectroscopy measurements. Baking on hot plate for 8 min at 80 °C followed by 2 min at 120 °C evaporates all traces of solvent and activates the NP formation. While the AuNP load on the composite could be controlled by the amount of gold salt added to the polymer, the layer thickness was defined by the proportion of PGMEA. It was verified that a 70:30 proportion of PGMEA on AZ9260 at the former spin coating conditions led to uniform layers with thickness in the 150–250 nm range.

The gold load in each sample was expressed as the mass fraction of gold salt on the commercial AZ9260 as weighted for the solution preparation, ignoring further additional solvent. However, AZ9260 is specified to contain already a 60–65 % wt. of solvents which are eliminated during soft bake. The relationship between the gold salt mass fraction and the final gold NP volume fraction is shown in Table 1. Uncertainties around 12 % in the mass fraction are mainly due to the uncertainty in the polymer concentration in AZ9260, while an additional 8 % uncertainty in the volume fraction is caused by the errors accumulated in the measurement of the polymer density. For simplicity, the composites will be called by their nominal gold salt initial concentration.

Characterization

Ellipsometric measurements were performed in the 0.59–4.43 eV spectral range with a phase-modulated ellipsometer (UVISEL, Horiba). The ellipsometric parameters I_s and I_c were measured at three angles of incidence: 50, 60, and 70°. These parameters depend on the ellipsometric angles Ψ and Δ:

$$I_s = \sin 2\Psi \sin \Delta, \tag{1}$$

$$I_c = \sin 2\Psi \cos \Delta. \tag{2}$$

TEM images are recorded with a Technai CM200 microscope operating at 200 kV. To prepare TEM grids, the films are stripped off the substrate by scratching the samples with a razor blade. The film fragments are then deposited on a copper TEM grid.

Extinction measurements are made with a home-made downright microscope. The sample is irradiated with a tungsten lamp. The angle of incidence is set at 0°. The transmitted light is collected with a 10× (NA: 0.3) microscope. The light is then focalized in the core of an optical fiber connected to a CCD spectrophotometer (Maya 2000pro UV–visible detector). For absorption spectroscopy, films are deposited on glass substrates. The reference intensity I_0 is measured after a glass substrate. Then, the light intensity I is measured by replacing the glass substrate by the sample. The extinction of the film is estimated by calculating the logarithm of the ratio I_0/I, neglecting the reflection at each interface. The extinction at plasmon resonance is then normalized to 1.

Shape-distributed effective medium theory (SDEMT)

In the following, we consider a collection of spheroidal NPs distributed in shape and randomly oriented in a polymer matrix. This medium is considered as a homogeneous medium described by an effective dielectric function ε_{eff}. The random orientation of NPs suggests that this effective medium is isotrope. In mean field approximation, the spatial averages of electric $\langle \mathbf{E} \rangle$ and displacement $\langle \mathbf{D} \rangle$ fields in the material are the sum of two contributions (Bohren and Huffman 1998):

$$\langle \mathbf{E} \rangle = (1-f)\langle \mathbf{E_m} \rangle + f\langle \mathbf{E_{np}} \rangle, \tag{3}$$

Table 1 Nominal gold mass and the corresponding nominal Au volume fraction for each formulation

Nominal $HAuCl_4$ concentration (% wt)	Nominal f_{NP} (% vol)	f_{NP} from ellipsometry (% vol)
5	0.6 ± 0.1	0.7 ± 0.05
10	1.0 ± 0.2	1.2 ± 0.05
20	2.2 ± 0.4	2.3 ± 0.08
40	6 ± 1	7 ± 0.1
60	12 ± 2	11 ± 0.1

The volume fraction of gold NPs deduced from ellipsometry is also reported

$$\langle \mathbf{D} \rangle = (1-f)\varepsilon_m \langle \mathbf{E_m} \rangle + f\varepsilon_{np} \langle \mathbf{E_{np}} \rangle, \tag{4}$$

where f is the NPs volume fraction, while $\langle \mathbf{E_m} \rangle$ and $\langle \mathbf{E_{np}} \rangle$ are the spatial average electric field inside the matrix and NPs, respectively. ε_{np} and ε_m are the complex dielectric function of NPs and the matrix, respectively. The effective dielectric function ε_{eff} is defined by

$$\langle \mathbf{D} \rangle = \varepsilon_{eff} \langle \mathbf{E} \rangle. \tag{5}$$

In the quasi-static limit i.e., for NP size smaller than the wavelength, the field inside the matrix is proportional to the field inside NPs.

$$\langle \mathbf{E_{np}} \rangle = \beta \langle \mathbf{E_m} \rangle. \tag{6}$$

The slope β is defined by (Resano-Garcia et al. 2015)

$$\beta = \frac{\varepsilon_m}{3} \int\int P(L_1, L_2) \sum_{i=1}^{3} \frac{1}{\varepsilon_m + L_i(\varepsilon_{np}(l) - \varepsilon_m)} \mathrm{d}L_1 \mathrm{d}L_2. \tag{7}$$

The depolarization parameters (L_1, L_2, L_3) which only depend on the NP shape vary in the 0–1 range and must respect the following sum rule:

$$1 = L_1 + L_2 + L_3. \tag{8}$$

P(L_1, L_2) is the normalized distribution of NP depolarization factors. We assume that the depolarization parameters follow a Gaussian distribution (Battie et al. 2014a, 2015; Resano-Garcia et al. 2015):

$$P(L_1, L_2) = C e^{-0.5\left(\frac{(L_1-\bar{L}_1)^2}{\sigma_1^2} + \frac{(L_2-\bar{L}_2)^2}{\sigma_2^2} + \frac{(L_3-\bar{L}_3)^2}{\sigma_3^2}\right)}. \tag{9}$$

Note that other distributions can be used. The distribution of NP depolarization factors is related to the NP shape distribution. $\bar{L}_i$ and σ_i are the mean value and standard deviation of L_i, respectively, while C is a constant used to normalize the distribution. To make easier the interpretation, we adopt the Bohren convention (Bohren and Huffman 1998): $L_1 \leq L_2 \leq L_3$.

The effective dielectric function of a medium composed of ellipsoidal NPs embedded in a dielectric matrix can be calculated from Eqs. (3–6):

$$\varepsilon_{eff} = \frac{(1-f)\varepsilon_m + f\varepsilon_{np}\beta}{(1-f) + f\beta}. \tag{10}$$

Note that the volume fraction must be small enough to neglect the interaction between NPs (Evlyukhin et al. 2012; Hohenester and Krenn 2005; Ranjan 2013; Yousif and Samra 2013). The dielectric function of bulk Au (ε_{bulk}) (Palik 1985) is related to the contribution of interband and intraband transitions of bound and conduction electrons, respectively (Kreibig and Vollmer 1995). The intraband transitions are described by the Drude dispersion law (Kreibig and Vollmer 1995). In a classical limit, intrinsic confinement occurs for NP size smaller than the mean-free path of conduction electrons. By assuming that the intrinsic confinement only affects free electrons, the dielectric function of AuNPs can be deduced from

$$\varepsilon_{np}(l) = \varepsilon_{bulk} - \frac{\omega_p^2}{\omega(\omega + i\Gamma_0)} + \frac{\omega_p^2}{\omega\left(\omega + i\left(\Gamma_0 + A\frac{v_f}{l}\right)\right)}, \tag{11}$$

where ω is the photon energy and A a constant. $\omega_p = 8.64$ eV, $\Gamma_0 = 0.097$ eV, and $v_f = 1.4{*}10^6$ m/s are the bulk plasma energy, the bulk electron damping and the Fermi velocity of free electrons, respectively. l is the mean value of NP size. The value of the constant A is still under debate and depends on the scattering scheme (Coronado and Schatz 2003; Kreibig and Vollmer 1995), the NP shape (Coronado and Schatz 2003), and the chemical environment (Charlé et al. 1984; Hövel et al. 1993; Kreibig 2008). As example, in the case of spherical NPs in vacuum, an isotropic electron scattering leads to $A = 1$ while $A = 0.75$ for a Lambert cosine scattering law (Coronado and Schatz 2003), both being significantly higher than the experimental result for 2 nm AgNP in vacuum of $A = 0.25$ (Hövel et al. 1993).

Results and discussion

Figure 1 shows typical TEM images of AuNP films and the corresponding diameter distributions measured over 300 NPs. In the following, the diameter is defined as the mean value between the smaller and larger apparent dimensions of each NP. Since the thickness of the film chips obtained during the TEM grid preparation is not controlled, the concentration of NPs cannot be estimated by TEM. Indeed, TEM images show juxtaposition of AuNPs located at different film depths. In other words, the interparticle distance cannot be evaluated from TEM measurements. In first approximation, the NP diameter distribution follows a Gaussian distribution. To avoid negative diameter value, we limit the representation of the Gaussian distribution to diameter higher than 1 nm which approximately corresponds to the resolution limit of TEM.

Au5, Au10, and Au20 have similar NP diameter distributions centered close to 4 nm with 1 nm standard deviation. The Au40 diameter distribution has a slightly larger width estimated at 1.5 nm. On the other hand, the Au60 diameter distribution is drastically broadened while its mean diameter is 3 times higher than the Au5 one. In all cases, the NP diameter is smaller than the 42 nm electron mean-free path of bulk Au (Kreibig and Vollmer 1995).

The NPs aspect ratio distributions reported in Fig. 2 enable a quantitative estimation of the NP shape distribution. In the following, the NP aspect ratio is defined as the ratio between the lower and the higher NP diameter. Au5, Au10, and Au20 mainly contain spherical NPs. However, the amount of spherical NPs tends to decrease from 86 to 30 % as the gold precursor concentration increases from 5 to 60 %. Indeed, as shown in the TEM image (Fig. 1e), Au60 is mainly composed of elongated NPs which come from the coalescence of NPs. These NPs are randomly oriented inside the photoresist film. Note that the proportion of spherical NPs deduced from TEM measurements should be overestimated since elongated NPs in one direction can appear as nearly spherical NPs, depending on their orientation.

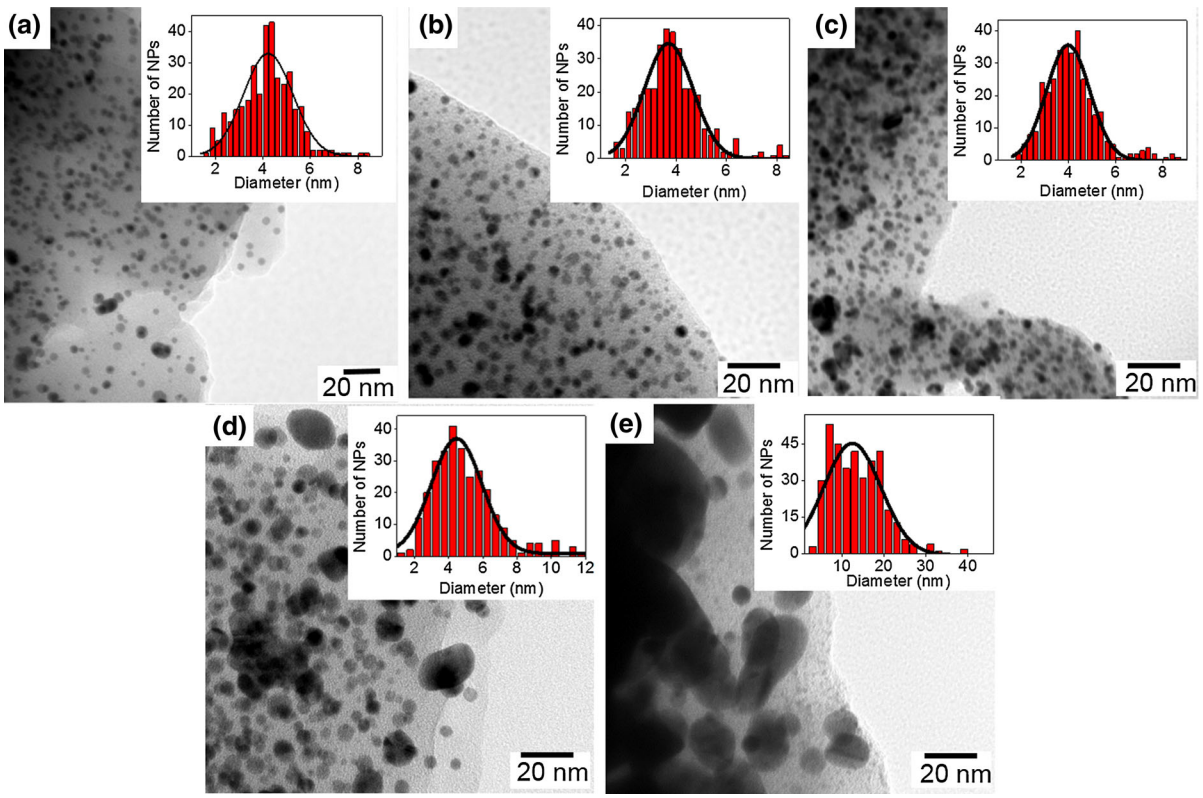

Fig. 1 TEM images of **a** Au5, **b** Au10, **c** Au20, **d** Au40 and **e** Au60. In *inset* the corresponding NP diameter distributions

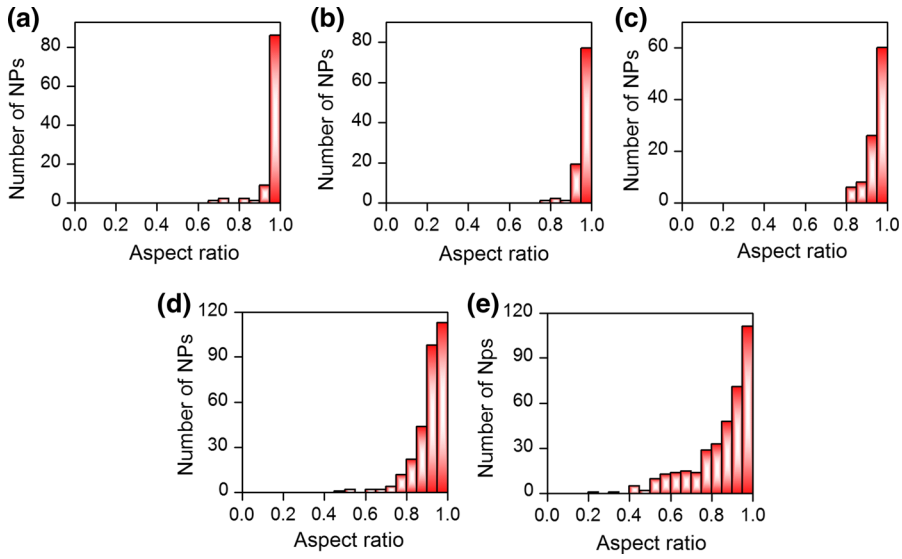

Fig. 2 NP aspect ratio distribution of **a** Au5, **b** Au10, **c** Au20, **d** Au40 and **e** Au60

Spectroscopic ellipsometric measurements of Au20 are illustrated in Fig. 3. Similar spectra are obtained for other films (not shown). To extract optical properties of nanocomposite layers from ellipsometric data, an optical model must be introduced. This model consists of a silicon substrate covered with a photoresist film which contains AuNPs.

The optical properties of these films are described by an effective dielectric function calculated from Eq. (10). In agreement with the quasi-static approximation, the NP size deduced from TEM measurements is much smaller than the wavelength. In other words, multipolar and dynamic effects are negligible for this NP size (Battie et al. 2014b). In addition, by considering the nominal NP volume fraction (Table 1), the interparticle distance is sufficiently high to neglect the interaction between NPs. The dielectric function of the matrix ε_m is set to the value measured on a photoresist film without gold precursor. The transfer matrix formalism (Azzam and Bashara 1977) is then used to calculate the ellipsometric parameters (I_s, I_c). The mean values ($\bar{L}_1$, $\bar{L}_2$) and standard deviations of (σ_1, σ_2, σ_3) of the distribution of depolarization factors, the NP volume fraction f, the ratio A/l, and the film thickness have been simultaneously fitted using the Levenberg–Marquard algorithm (Levenberg 1944). These parameters are summarized in Tables 1 and 2.

As shown in Fig. 3, a good agreement is obtained between the experimental spectra and the calculated ones. The root mean square error between the experimental and the simulated data does not exceed 0.06 for all films (spectra not shown), confirming the correctness of this model. Moreover, the correlation matrix

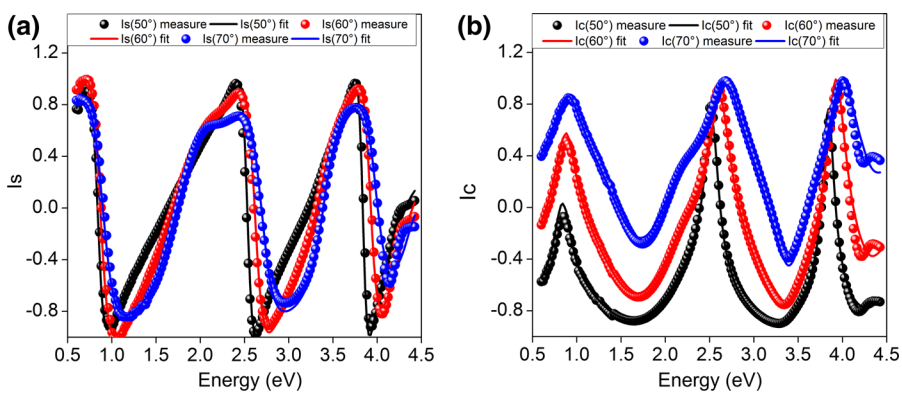

Fig. 3 Measured and calculated **a** *I*s, **b** *I*c ellipsometric spectra of Au20. The angles of incidence are 50, 60, and 70°

Table 2 Parameters of the NP shape distributions and A/*l* values deduced from ellipsometry for all nominal $HAuCl_4$ concentration

Nominal $HAuCl_4$ concentration (% wt)	$\bar{L}_1$	$\bar{L}_2$	σ_1	σ_2	σ_3	A/l (nm^{-1})
5	0.330 ± 0.005	0.332 ± 0.005	0.042 ± 0.003	0.013 ± 0.002	0.021 ± 0.003	0.72 ± 0.02
10	0.33 ± 0.01	0.33 ± 0.01	0.014 ± 0.005	0.015 ± 0.006	0.02 ± 0.008	0.71 ± 0.04
20	0.318 ± 0.006	0.328 ± 0.008	0.013 ± 0.004	0.012 ± 0.004	0.022 ± 0.006	0.73 ± 0.02
40	0.320 ± 0.005	0.321 ± 0.005	0.089 ± 0.005	0.065 ± 0.004	0.021 ± 0.001	1.02 ± 0.05
60	0.22 ± 0.02	0.35 ± 0.01	0.017 ± 0.002	0.851 ± 0.009	0.078 ± 0.003	0.48 ± 0.02

(not shown) suggests that all free parameters are independent. The NP volume fractions deduced from ellipsometry (Table 1) are close to the nominal values, suggesting that the gold salt is completely reduced during the heat treatment. This model is limited to small NP volume fraction to neglect the interaction between NPs. The maximum value for which this model remains valid has not reached a consensus yet. Myroshnychenko et al. (2008) have suggested that the volume fraction must be smaller than 30 %. On the other hand, as reported by Kreibig et al. (1995), the dipolar interaction is negligible for volume fraction smaller than 5 %. Although the volume fraction of Au60 is slightly larger than this threshold, we assume that Au60 is only slightly affected by dipolar interactions. In other words, we consider that Au60 is at the edge of SDEMT applicability.

The distributions of NP depolarization factor P(L_1, L_2) deduced from ellipsometry are reported in Fig. 4. Au5, Au10, and Au20 have narrow depolarization factor distribution centered close to (1/3, 1/3) suggesting that AuNPs are spherical for $HAuCl_4$ concentration lower than 20 %. The distributions of depolarization factors are broadened for $HAuCl_4$ concentrations higher than 40 %. Moreover, the mean values of depolarization factors deviate from that of spherical NPs.

By assuming that film contains ellipsoidal NPs, the distribution of depolarization factor P(L_1, L_2) illustrated in Fig. 4 can be converted into a distribution P(r_2, r_3) in aspect ratios of ellipsoidal NPs by applying the following space transformation (Bohren and Huffman 1998):

$$L_i = \frac{r_2 r_3}{2} \int_0^{+\infty} \frac{dq}{(q + r_i^2)\sqrt{\prod_{i=1}^{3}(q + r_i^2)}}, \qquad (12)$$

where $r_i = a_i/a_1$ (i = 1, 2, 3) the aspect ratios of an ellipsoidal NP. a_1, a_2,and a_3 are the length of principal axes of the ellipsoidal NP. To obtain a bijective space, the lengths of principal axes are sorted in the following order: $a_3 \leq a_2 \leq a_1$. The NP aspect ratios distributions are depicted in Fig. 5.

In accordance with the NP aspect ratio distribution found by TEM (Fig. 2), Au5, Au10, and Au20 are mainly composed of spherical NPs. Indeed, their aspect ratios r_2 and r_3 are close to 1. The distributions of aspect ratios are broadened for Au40 and Au60. In addition, the Au60 aspect ratio distribution is centered at the (0.68, 0.57) values confirming the nonsphericity of NPs. This also suggests that the NP shape is close to prolate since the mean value of r_2 is close to the mean value of r_3. TEM measurements reveal that the nanoparticles aspect ratio is in the 0.4–1 range. However, a large number of NPs with an aspect ratio close to 1 is observed by TEM. TEM gives a two-dimensional projection of NPs. Indeed, only one aspect ratio per NP can be measured by TEM. In other words, the aspect ratio estimated by TEM can be overestimated because nonspherical elongated nanoparticles could appear as closely spherical NPs, depending on their orientation. In other words, TEM can overestimate the amount of spherical NPs.

To quantify the variations of NP shape distribution, we introduced the sphericity parameter P_s and the dispersity parameter D:

$$P_s = \sqrt{\sum_{i=1}^{3}\left(\bar{L}_i - \frac{1}{3}\right)^2}, \qquad (13)$$

$$D = \frac{1}{\sqrt{\sum_{i=1}^{3}\frac{1}{\sigma_i^2}}}. \qquad (14)$$

P_s is the Euclidian distance between the center of the depolarization factor distribution and the locus of spherical NPs. It varies in the 0–0.82 range. The sphericity parameter of monodispersed spherical NPs

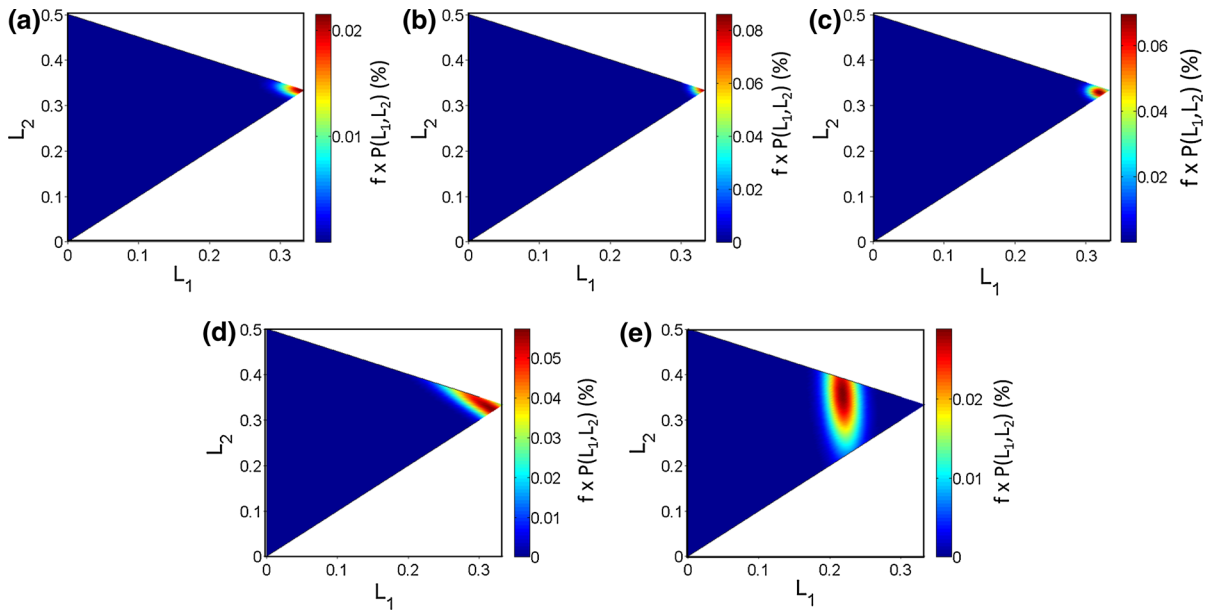

Fig. 4 P(L_1,L_2) distribution of **a** Au5, **b** Au10, **c** Au20, **d** Au40 and **e** Au60

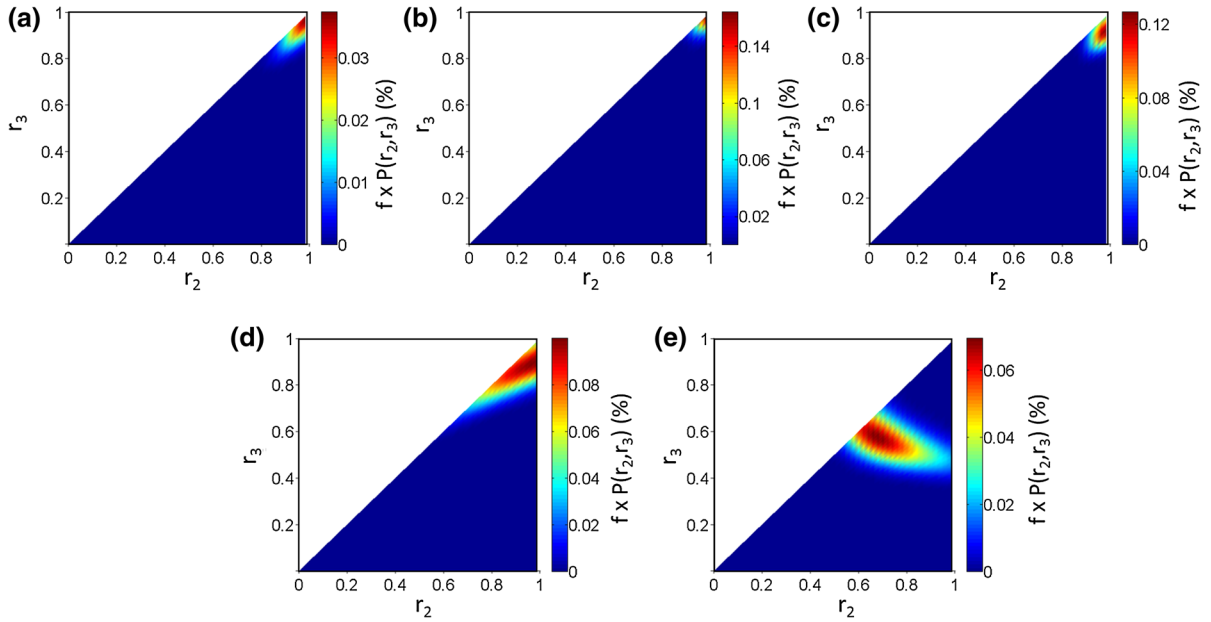

Fig. 5 Distribution of NP aspect ratios P(r_2,r_3) of **a** Au5, **b** Au10, **c** Au20, **d** Au40 and **e** Au60

should be equal to 0. However, SDEMT does not take into account multipolar effects which appear for large NP radius (Kreibig and Vollmer 1995). To give a better sphericity criterion, spectra of spherical NPs simulated from Mie theory (Bohren and Huffman 1998) are fitted with the SDEMT (not shown). We conclude that the spherical NPs with a diameter smaller than 50 nm have a sphericity parameter smaller than 0.03. The dispersity parameter evaluates the width of the shape distribution. As example, monodispersed NPs have a D value close to 0. Figure 6 reports the variations of sphericity and

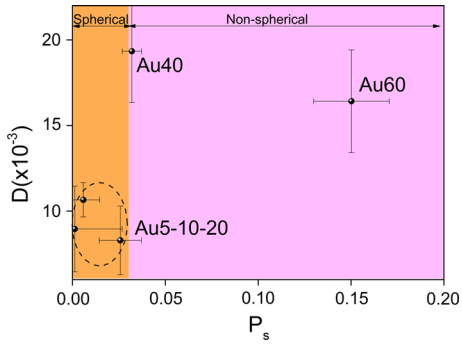

Fig. 6 Dispersity parameter versus the sphericity parameter for each $HAuCl_4$ concentration

dispersity with the $HAuCl_4$ concentration. The dispersity parameter remains approximately constant for $HAuCl_4$ concentration smaller than 20 %, while it drastically increases for higher concentrations. In addition, the sphericity parameters of Au5, Au10, and Au20 are lower than 0.03 confirming that these films are mainly composed of spherical NPs. The Au40 sphericity parameter is close to the spherical shape criterion threshold. However, it has a high dispersity parameter estimated at 0.019. The Au60 sphericity parameter and dispersity parameter are 0.15 and 0.017, respectively. In other words, Au40 and Au60 have broad NP shape distributions. Indeed, TEM images suggest that both films are composed of a mixture of spherical NPs, elongated NPs and faceted large NPs. The variations of the NP shape distribution with the Au concentration can be explained by considering two mechanisms: the nucleation and the coalescence of NPs. In a low concentration regime, the NP growth mechanism is governed by the reduction of Au salt and the nucleation of isolated spherical NPs. A small rise of Au salt concentration increases the number of nucleation centers, i.e. the number of NPs, without changing their radius distribution. Then, the coalescence of NPs appears for a gold precursor concentration higher than 40 %. This induces the growth of large nonspherical NPs.

The NP mean radius obtained by TEM (Fig. 1) is smaller than the 42 nm electron mean-free path of Au (Kreibig and Vollmer 1995). In other words, the scattering of electrons on the NP surface limits their mean-free path. Ellipsometry cannot give a direct estimation of A parameter without the knowledge of nanoparticle radius. Thus, we combine ellipsometric measurements and TEM to give an estimation of A. The constant A is calculated from the product between the ellipsometric estimation of A/*l* and the NP mean radius deduced from TEM. Figure 7 reports the calculated A parameter as a function of the sphericity and dispersity parameters. The magnitude of the A error bars is calculated by taking into account the error on A/*l* deduced from the fitting procedure and the standard deviation of NP radius distribution obtained from TEM. For a sphericity parameter smaller than 0.03, i.e., for nearly spherical NPs, the A parameter collapses to the 1.42 ± 0.26 value. As reported by several authors (Charlé et al. 1984; Coronado and Schatz 2003; Hövel et al. 1993; Kreibig 2008; Kreibig and Vollmer 1995), the A parameter of spherical NPs in vacuum or in air is smaller than 1. However, for embedded NPs, an energy transfer between the NP and its matrix can occur for a plasmon energy close to the adsorbate energy levels (Charlé et al. 1984; Hövel et al. 1993; Kreibig 2008). This chemical interface damping, which reflects the chemical and structural properties at the NP–matrix interface, damps the phase coherence of the collective oscillation. As example, Hövel et al. (1993), Kreibig (2008) and Kreibig and Vollmer (1995) have reported a value A of 1.4 for silver NPs embedded in silica matrix. In other words, the chemical damping plays a major rule in the optical properties of small spherical NPs embedded in photoresist film. On the other end, Au40 and Au60 which have broad NP size and shape distributions have A parameter larger than 2. The A parameter depends on the plasmon band width. Since SDEMT does not take into account inhomogeneous broadening due to the NP size distribution, the A parameter can be slightly overestimated. This inhomogeneous broadening should be more pronounced for larger NP diameter such as Au40 and Au60 as illustrated by the high magnitude of their A error bar. In addition, as reported by Coronado and Schatz (2003), the A parameter is shape and aspect ratio dependent. As example, the A parameter of oblate NPs in vacuum varies in the 0.25–1.7 range. Moreover, the high error bars of the A parameter of Au40 and Au60 are related to their broad NP size distributions. Indeed, the size distribution, which can induce inhomogeneous broadening of the SPR bands, is not taken into account in SDEMT. In other words, the high A parameter value of Au40 and Au60 is due to their broad NP size and shape

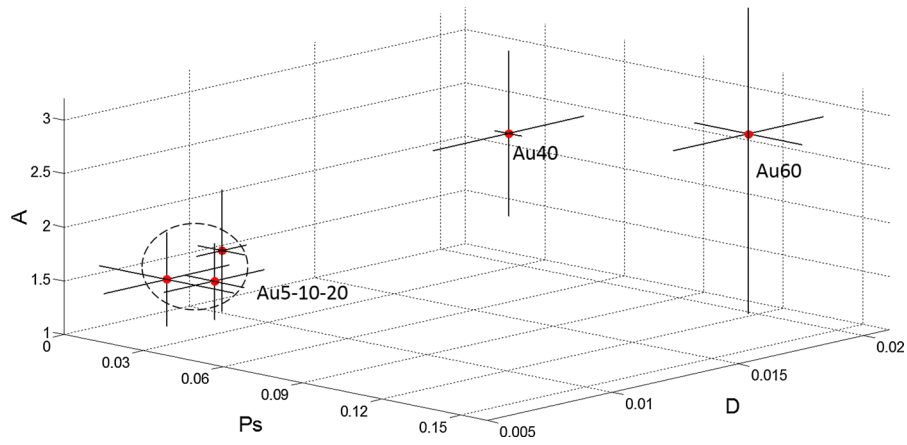

Fig. 7 Influence of the sphericity and dispersity parameters on the value A

distributions and the deviation of the NP shape from spherical NPs.

The NP shape distribution has a strong influence on their optical properties. Figure 8a and b shows the real part and the imaginary part of the effective dielectric function of films. The effective absorption coefficients of the photoresist/AuNP films calculated from the effective dielectric functions and the normalized absorption measured by absorption spectroscopy are also reported in Fig. 8c and d. Note that due to the random orientation of NPs, the AuNPs/photoresist film is described as an isotropic effective medium. The complex dielectric function of the photoresist matrix is also reported. The matrix is transparent below 3.6 eV while it has a nonnegligible absorption for higher energy. The contribution of 5d → 6sp interband transitions of AuNPs is traduced by a nearly constant imaginary part of the effective dielectric function in the 2.7–4 eV range which increases with the Au concentration. The imaginary part of dielectric function and the absorption coefficient exhibit a strong asymmetric SPR band located in the 2–2.5 eV range. In accordance with the Kramers–Kronig relations (Kronig 1926), a large variation of the real part of the effective dielectric function occurs close to the resonance. The absorption coefficient calculated using the effective dielectric function deduced from ellipsometry is in agreement with the normalized absorption measured by absorption spectroscopy (Fig. 8c) confirming the correctness of the ellipsometric model. The small differences between the spectra obtained by absorption spectroscopy and ellipsometry are due to the fact that both measurements are made on different samples. Indeed, contrary to ellipsometry, absorption measurement cannot be performed on nontransparent substrate. In addition, the determination of absorption coefficient from absorption spectroscopy requires the knowledge of film thickness, and the losses, due to the reflection at each air/film and film/substrate interfaces, are not taken into account in absorption spectroscopy. Moreover, the complex dielectric function, which is a crucial parameter to design optical devices such as waveguides, or metamaterials cannot be extracted by absorption spectroscopy. Although the volume fractions are different, the dielectric functions of Au10 and Au20 are close together confirming that the polarization state of light is sufficiently sensitive to detect small variations of the complex dielectric function. The SPR energy of Au5, Au10, and Au20 is 2.25 eV. In accordance with the Fröhlich relation (Kreibig and Vollmer 1995), this band is assimilated to the SPR band of spherical NPs. The SPR band is redshifted from 2.25 to 2 eV, while its full width at half maximum increases by 1.5 times when the Au precursor concentration evolves from 20 to 60 %. By considering the low NP size obtained from TEM (Fig. 1), these spectral variations cannot be due to multipolar and dynamic effects which are observed for NPs size diameter than 50 nm (Battie et al. 2014b). Moreover, the NPs volume fraction (Table 1) is too small to attribute this redshift to the interaction effects. Thus, these variations come from the evolution of NPs shape with the gold precursor concentration. Moreover, a shoulder attributed to the transversal SPR mode of nonspherical NPs is observed at 2.2–2.3 eV in the effective absorption coefficient and the measured absorption spectra of Au60 (Fig. 8c, d). The SPR energy and bandwidth are mainly influenced by the

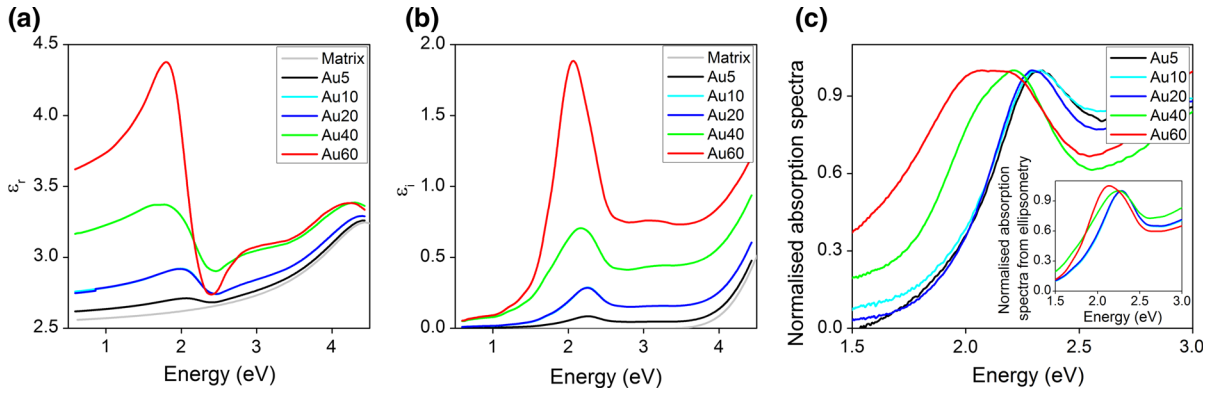

Fig. 8 **a** Real part and **b** imaginary part of the effective dielectric function of AuNPs/photoresist films. The dielectric function of the photoresist matrix is also reported. **c** Normalized absorption spectra of films deposited on glass substrate measured by absorption spectroscopy. In inset, normalized effective absorption coefficient of the photoresist/AuNP films calculated using the effective dielectric function deduced from ellipsometry

mean value and the width of the depolarization factor distribution, respectively (Resano-Garcia et al. 2015). In order words, the high NP shape dispersity in Au40 or Au60 induces an inhomogeneous broadening of the plasmon band.

Conclusions

In summary, we have introduced an effective medium theory which takes into account the intrinsic confinement effect and the distribution of NPs shape. This theory has been used to analyze ellipsometric spectra recorded on photoresist films which contain AuNPs. This theory is valid for low volume fraction. The A parameter is matrix and shape dependent suggesting that the absolute size of NPs cannot be determined from ellipsometric measurements. However, the NP shape distributions and volume fraction are extracted from ellipsometric measurements. Contrary to TEM measurements, the NP shape distribution is obtained from a large number of NPs. Indeed, by considering the ellipsometric beam diameter, the film thickness, and the NP volume fraction, we can conclude that the light beam probes approximately 10^{11} NPs. Moreover, contrary to TEM measurements, ellipsometry is a nondestructive technique which gives the dielectric function of nanocomposite film. Thus, we demonstrate that ellipsometry combined with SDEMT is an inexpensive alternative for TEM to estimate the NPs shape distribution.

Acknowledgments Financial support of the "Conseil régional Champagne-Ardenne", NanoMat (http://www.nanomat.eu) by the "Ministère de l'enseignement supérieur et de la recherche" is acknowledged.

References

Aldeanueva-Potel P, Faoucher E, Alvarez-Puebla RA, Liz-Marzán LM, Brust M (2009) Recyclable molecular trapping and SERS detection in silver-Loaded agarose gels with Dynamic hot spots. Anal Chem 81:9233–9238

Azzam RMA, Bashara NM (1977) Ellipsometry and Polarized Light. North-Holland Publishing Company, Amsterdam

Battie Y, Destouches N, Chassagneux F, Jamon D, Bois L, Moncoffre N, Toulhoat N (2011) Optical properties of silver nanoparticles thermally grown in a mesostructured hybrid silica film. Opt Mater Express 1:1019–1033

Battie Y, En Naciri A, Chamorro W, Horwat D (2014a) Generalized effective medium theory to extract the optical properties of two-dimensional nonspherical metallic nanoparticle layers. J Phys Chem C 118:4899

Battie Y, Resano-Garcia A, Chaoui N, Zhang Y, En Naciri A (2014b) Extended Maxwell-Garnett-Mie formulation applied to size dispersion of metallic nanoparticles embedded in host liquid matrix. J Chem Phys 140:044705

Battie Y, Resano-Garcia A, En Naciri A, Akil S, Chaoui N (2015) Determination of morphological characteristics of metallic nanoparticles based on modified Maxwell-Garnett fitting of optical responses. Appl Phys Lett 107:143104

Biswas A, Aktasa OC, Kanzowa J, Saeeda U, Strunskusb T, Zaporojtchenkoa V, Faupela F (2004) Polymer-metal optical nanocomposites with tunable particle plasmon resonance prepared by vapor phase co-deposition. Mater Lett 58:1530–1534

Bohren CF, Huffman DR (1998) Absorption and scattering by a sphere. In: absorption and scattering of light by small particles. Wiley, Weinheim

Charlé KP, Frank F, Schulze W (1984) The optical properties of silver microcrystallites in dependance on size and the influence of the matrix environment. Ber Bunsenges Phys Chem 88:350

Coronado EA, Schatz GC (2003) Surface plasmon broadening for arbitrary shape nanoparticles: A geometrical probability approach. J Chem Phys 119:3926–3934

Destouches N, Battie Y, Crespo-Monteiro N, Chassagneux F, Bois L, Bakhti S, Vocanson F, Toulhoat N, Moncoffre N, Epicier T (2013) Photo-directed organization of silver nanoparticles in mesostructured silica and titania films. J Nanopart Res 15:1–10

Evlyukhin AB, Reinhardt C, Urs Zywietz U, Chichkov BN (2012) Collective resonances in metal nanoparticle arrays with dipole-quadrupole interactions. Phys Rev B 85:245411

Gao L, Li Z (2003) Effective medium approximation for two-component nonlinear composites with shape distribution. J Phys: Condens Matter 15:4397

Goncharenko AV (2003) Generalizations of the Bruggeman equation and a concept of shape-distributed particle composites. Phys Rev E 68:041108

Goncharenko AV (2004) Spectral density function approach to homogenization of binary mixtures. Chem Phys Lett 400:462–468

Goncharenko AV, Pinchuk AO (2014) Broadband epsilon-near-zero composites made of metal nanospheroids. Opt Mater Express 4:1276–1286

Goncharenko AV, Venger EF (2004) Percolation threshold for Bruggeman composites. Phys Rev E 70:057102

Goncharenko AV, Lozovski VZ, Venger EF (2001) Effective dielectric response of a shape-distributed particle system. J Phys: Condens Matter 13:8217

Gradess R, Abargues R, Habbou A, Canet-Ferrer J, Pedrueza E, Russell A, Valdés JL, Martínez-Pastor JP (2009) Localized surface plasmon resonance sensor based on Ag-PVA nanocomposite thin films. J Mater Chem 19:9233–9240

Guzatov DV, Vaschenko SV, Stankevich VV, Lunevich AY, Glukhov YF, Gaponenko SV (2012) Plasmonic enhancement of molecular fluorescence near silver nanoparticles: theory, modeling, and experiment. J Phys Chem C 116:10723–10733

Hedayati MK, Javaherirahim M, Mozooni B, Abdelaziz R, Tavassolizadeh A, Chakravadhanula VSK, Zaporojtchenko V, Strunkus T, Faupel F, Elbahr M (2011) Design of a perfect black absorber at visible frequencies using plasmonic metamaterials. Adv Mater 23:5410–5414

Hohenester U, Krenn J (2005) Surface plasmon resonances of single and coupled metallic nanoparticles: A boundary integral method approach. Phys Rev B 72:195429

Hövel H, Fritz S, Hilger A, Kreibig U, Vollmer M (1993) Width of cluster plasmon resonances: bulk dielectric functions and chemical interface damping. Phys Rev B 48:18178

Ishikawa A, Tanaka T (2012) Two-photon fabrication of three-dimensional metallic nanostructures for plasmonic metamaterials. J Laser Micro Nanoen 7:11–15

Keita AS, Naciri AE (2011) Size distribution dependence of the dielectric function of Si quantum dots described by a modified Maxwell-Garnett formulation. Phys Rev B 84:125436

Keita AS, En Naciri A, Battie Y, Delachat F, Carrada M, Ferblantier G, Slaoui A (2014) Determination of the optical properties and size dispersion of Si nanoparticles within a dielectric matrix by spectroscopic ellipsometry. J Appl Phys 116:103520

Kinnan MK, Kachan S, Kn Simmons C, Chumanov G (2009) Plasmon coupling in two-dimensional arrays of silver nanoparticles: I. effect of the dielectric medium. J Phys Chem C 113:7079–7084

Kreibig U (2008) Interface-induced dephasing of Mie plasmon polaritons. Appl Phys B 9:79–89

Kreibig U, Vollmer M (1995) Optical properties of metal clusters. Berlin, Springer

Kronig RDL (1926) On the theory of the dispersion of X-rays. J Opt Soc Am 12:547–557

Kubacka A, Cerrada ML, Serrano C, Fernández-García M, Ferrer M, Fernández-Garcia M (2009) Plasmonic nanoparticle/polymer nanocomposites with enhanced photocatalytic antimicrobial properties. J Phys Chem C 113:9182–9190

Kuila BK, Garai A, Nandi AK (2007) Synthesis, optical, and electrical characterization of organically soluble silver nanoparticles and their poly(3-hexylthiophene) nanocomposites: Enhanced luminescence property in the nanocomposite thin films. Chem Mater 19:5443–5452

Levenberg KA (1944) Method for the solution of certain problems in least squares. Q Appl Math 2:164–168

Liu Y, Mills EN, Composto RJ (2009) Tuning optical properties of gold nanorods in polymer films through thermal reshaping. J Mater Chem 19:2704–2709

Losurdo M, Bergmair M, Bruno G, Cattelan D, Cobet C, De Martino A, Feischer K, Dohceviv-Mitrovic Z, Esser N, Galliet M, Gajic R, Hemzal D, Hingerl K, Humlicek J, Ossikovski R, Popovic ZV, Saxl O (2009) Spectrocopic ellipsometry and polarimetry for materials and systems analysis at the nanometer scale: state of the art potential, and perspectives. J Nanopart Res 11:1521–1554

Marques-Hueso J, Abargues R, Valdés JL, Martínez-Pastor JP (2010) Ag and Au/DNQ-novolac nanocomposites patternable by ultraviolet lithography: a fast route to plasmonic sensor microfabrication. J Mater Chem 20:7436–7443

Misra N, Kumar V, Goel NK, Varshney L (2015) Radiation synthesized poly(n-vinyl-2-pyrrolidone)-stabilized-gold nanoparticles as LSPR-based optical sensor for mercury ions estimation. J Nanopart Res 7:279

Myroshnychenko V, Rodrıguez-Fernandez J, Pastoriza-Santos I, Funston AM, Novo C, Mulvaney P, Liz-Marzan LM, Garcıa de Abajo FJ (2008) Modelling the optical response of gold nanoparticles. Chem Soc Rev 37:1792–1805

Naciri AE, Miska P, Keita AS, Battie Y, Rinnert H, Vergnat M (2013) Optical properties of uniformly sized silicon nanocrystals within a single silicon oxide layer. J Nanopart Res 15:1–9

Oates TWH (2006) Real time spectroscopic ellipsometry of nanoparticle growth. Appl Phys Lett 88:213115

Oates TWH, Christalle E (2007) Real-time spectroscopic ellipsometry of silver nanoparticle formation in poly (vinyl alcohol) thin films. J Phys Chem C 111:182–187

Oates TWH, Mücklich A (2005) Evolution of plasmon resonances during plasma deposition of silver nanoparticles. Nanotechnology 16:2606

Oates TWH, Wormeester H, Arwin H (2011) Characterization of plasmonic effects in thin films and metamaterials using spectroscopic ellipsometry. Prog Surf Sci 86:328–376

Pacios R, Marcilla R, Pozo-Gonzalo C, Pomposo JA, Grande H, Aizpurua J, Mecerreyes D (2007) Combined electrochromic and plasmonic optical responses in conducting polymer/metal nanoparticle films. J Nanosci Nanotechnol 7:2938–2941

Palik ED (1985) Handbook of Optical Constants of Solids. Academic press handbook series, NewYork

Pandey S, Goswami GK, Nanda KK (2012) Green synthesis of biopolymer-silver nanoparticle nanocomposite: An optical sensor for ammonia detection. Int J Biol Macromol 51:583–589

Pecharroman C, Della Gaspera E, Martucci A, Escobar-Galindod R, Mulvaney P (2015) Determination of the optical constants of gold nanoparticles from thin-film spectra. J Phys Chem C 119:9450–9459

Persechini L, Verre R, McAlinden N, Wang JJ, Ranjan M, Facsko S, Shvets IV, McGilp JF (2014) An analytic approach to modeling the optical response of anisotropic nanoparticle arrays at surfaces and interfaces. J Phys: Condens Matter 26:145302

Qu S, Songa Y, Dub C, Wanga Y, Gaoa Y, Liua S, Lib Y, Zhu D (2004) Nonlinear optical properties in three novel nanocomposites with gold nanoparticles. Opt Comm 196:317–323

Ranjan M (2013) Predicting plasmonic coupling with Mie-Gans theory in silver nanoparticle arrays. J Nanopart Res 15:1908

Reddy KR, Lee KP, Lee Y, Gopalan AI (2008) Facile synthesis of conducting polymer-metal hybrid nanocomposite by in situ chemical oxidative polymerization with negatively charged metal nanoparticles. Mater Lett 62:1815–1818

Resano-Garcia A, Battie Y, En Naciri A, Akil S, Chaoui N (2015) Experimental and theoretical determination of the plasmonic responses and shape distribution of colloidal metallic nanoparticles. J Chem Phys 142:134108

Sandu T (2012) Shape effects on localized surface plasmons resonances in metallic nanoparticles. J Nanopart Res 14:905

Shukla S, Vidal X, Furlani EP, Swihart TM, Kim KT, Yoon YK, Urbas A, Prasad PN (2011) Subwavelength direct laser patterning of conductive gold nanostructures by simultaneous photopolymerization and photoreduction. ACS Nano 5:1947–1957

Takele H, Schürmann U, Greve H, Paretkar D, Zaporojtchenko V, Faupel F (2006) Controlled growth of Au nanoparticles in co-evaporated metal/polymer composite films and their optical and electrical properties. Eur Phys J App. Phys 33:83–89

Tamboli MS, Kulkarni MV, Patil RH, Gade WN, Navale SC, Kale BB (2012) Nanowires of silver-polyaniline nanocomposite synthesized via in situ polymerization and its novel functionality as an antibacterial agent. Colloid Surf B 92:35–41

Toudert J, Babonneau D, Simonot L, Cameli S, Girardeau T (2008) Quantitative modelling of the surface plasmon resonances of metal nanoclusters sandwiched between dielectric layers: the influence of nanocluster size, shape and organization. Nanotechnology 19:125709

Toudert J, Simonot L, Camelio S, Babonneau D (2012) Advanced optical effective medium modeling for a single layer of polydisperse ellipsoidal nanoparticles embedded in a homogeneous dielectric medium: surface plasmon resonances. Phys Rev B 86:045415

Yang P, Kawasaki K, Ando M, Murase N (2012) Au/SiO_2/QD core/shell/shell nanostructures with plasmonic-enhanced photoluminescence. J Nanopart Res 14:1025

Yousif BB, Samra AS (2013) Optical responses of plasmonic gold nanoantennas through numerical simulation. J Nanopart Res 15:1341